HHS Public Access

Author manuscript

*Magn Reson Imaging*. Author manuscript; available in PMC 2018 April 01.

Published in final edited form as:

*Magn Reson Imaging*. 2017 April ; 37: 273–281. doi:10.1016/j.mri.2016.11.023.

# Pharmacokinetic analysis and drug delivery efficiency of the focused ultrasound-induced blood-brain barrier opening in non-human primates

**Gesthimani Samiotaki**, **Maria Eleni Karakatsani**, **Amanda Buch**, **Stephanos Papadopoulos**, **Shih Ying Wu**, **Sachin Jambawalikar**, and **Elisa E. Konofagou**

## Abstract

**Purpose—**Focused Ultrasound (FUS) in conjunction with systemically administered microbubbles has been shown to open the Blood-Brain Barrier (BBB) locally, non-invasively and reversibly in rodents and non-human primates (NHP), suggesting the immense potential of this technique. The objective of this study entailed the investigation of the physiologic changes in the brain following the FUS-induced BBB opening and their relationship with the underlying anatomy.

**Materials and Methods—**Pharmacokinetic analysis was implemented in NHP's that received FUS at various acoustic pressures. Relaxivity mapping enabled the robust quantitative detection of the BBB opening as well as gray and white matter segmentation. Drug delivery efficiency was measured for pre-clinical validation of the technique.

**Results—**Based on our results, the opening volume and the amount of the gadolinium delivered were found mostly contained in the grey matter, while FUS-induced permeability and drug concentration varied depending upon the underlying brain inhomogeneity, and increased with the acoustic pressure.

**Conclusions—**Overall, apart from the *in vivo* protocols for BBB analysis developed here, this study also suggests the important role that FUS can have in efficient drug delivery via localized and transient BBB opening.

### Keywords

focused ultrasound; BBB opening; pharmacokinetics; relaxometry; concentration mapping

## 1. Introduction

The blood-brain barrier (BBB) presents a physical and metabolic barrier protecting the brain tissue, and thus excludes 98% of small molecule drugs and all large molecule drugs.

**Address correspondence to:** Maria Eleni Karakatsani, Department of Biomedical Engineering, Columbia University, 630W 168 St, Physicians and Surgeons 19-418, New York, NY, USA 10032, mek2204@columbia.edu, Tel: 212-342-1612.

Focused ultrasound (FUS) in conjunction with systemic administration of microbubbles has been established as the only method to disrupt the blood-brain barrier (BBB) locally, non-invasively and reversibly, in rodents and non-human primates. FUS-induced BBB opening allows the passive diffusion of molecules from the vasculature to the brain parenchyma, by increasing the permeability in the targeted region.

In non-human primates (NHP), the FUS-induced BBB opening has been studied using magnetic resonance imaging (MRI) [1]–[3] for the detection of the opening and any associated damage. In rodents, physiological properties of the BBB opening, such as permeability, volume, contrast agent concentration mapping and reversibility timeline, have been studied [4]–[7]; these studies provided invaluable bases for the optimal design for drug delivery to the brain using FUS, and *in vivo* tools for the quantification of the efficacy of this technique. However, other than the size, the NHP brain is not as homogeneous as the rodent brain, and it has been shown that the diffusion of contrast agents through the FUS-induced BBB opening in NHPs does not follow the same uniform pattern as in mice [1–3]. Subject-specific analysis that would allow taking into consideration the anatomy of each subject and the physiology of each brain, was thus rendered critical given the urgent need for clinical translation of the FUS technique for efficient and safe drug delivery.

In previously reported NHP studies, T1-weighted imaging was used for the BBB opening analysis, which provided very limited information on the physiologic changes in the brain, while the detection of opening was based upon subjective criteria inducing discrepancies among different studies [1–3]. In this study, magnetic resonance (MR) relaxivity mapping was introduced and validated as a robust and user-independent method for the detection of BBB opening following the intravenous injection of gadolinium. Gadolinium is an MR-contrast agent (MR-CA) which normally does not cross the BBB and was therefore used here as an opening-tracer. MR-CAs in principle decrease the relaxation times $T_1$ and $T_2$ of tissue due to interactions with surrounding water molecules and protons. It is therefore, mandatory to model these relaxation time changes due to CA interactions in order to quantify the CA concentration. In this study, a standard relaxometry technique for $T_1$ mapping [8] was implemented acquiring gradient-echo images with variable flip angles (VFA) with short TR. The VFA-based $T_1$ mapping was validated on a phantom with solutions of known $T_1$ values and provided $T_1$ value estimation with high accuracy and high spatial and temporal resolution. The difference in relaxivity pre- and post-MR-CA injection was expected to be detected only in areas where gadolinium could diffuse, which apart from the brain vasculature, is expected to be observed only where BBB is disrupted. Moreover, since grey matter and white matter have distinctive $T_1$ times, $T_1$ mapping was used as a robust method for BBB opening detection with grey and white matter segmentation.

Permeability mapping in rodents after FUS-induced BBB opening using MRI has provided further insight into the study of BBB opening, following the generalized Tofts and Kermode kinetic model [9], using a single $T_1$ value for the entire mouse brain and population-averaged arterial-input function (AIF). It has been shown that permeability increases with acoustic pressure in rodents and that DCE-MRI can be used as an in vivo evaluation tool for the efficacy of the procedure. For these reasons, in this study, a DCE-MRI sequence was designed and used to quantify permeability and further analyze the physiologic changes in

the brain following FUS-induced BBB disruption. The $T_1$ maps were also used in the DCE analysis for accurate modeling and measurement of the permeability changes at high spatial and temporal resolution, using subject-specific AIF in each experiment.

A critical aspect with clinical implications is the concentration and amount of drug or agent that can be delivered to different brain regions using FUS. The quantification of the amount of drug delivered across the BBB is rather challenging, and current techniques face limitations such as increased radiation when measured with PET-CT, or sacrifice of the animal in order to perform *post mortem* protein quantification. MRI, on the other hand, offers an *in vivo* tool for quantification of the MR-CA, which is used as model drug. The gadolinium MR-CA was used as a model drug that diffused in the brain parenchyma, and it also has a given relaxivity change rate per mol at a given magnetic field strength. The comparison of the $T_1$ times before and after gadolinium injection therefore provided quantitative CA concentration maps, which were used as a quantitative pharmacodynamic analysis. The integration of the amount of CA delivered in the entire BBB opening area was finally used for drug delivery efficiency estimation *in vivo* and non-invasively for the first time in NHPs for this technique.

The purpose of this study was the investigation of the physiologic properties of BBB opening in vivo in NHPs, in order to assess the efficiency of the FUS-induced BBB opening as a technique with therapeutic potential for neurodegenerative diseases such as Parkinson's disease. In order to achieve these aims, *in vivo* quantitative tools for safe and optimal drug delivery using FUS in a pre-clinical setting were developed and used following subject-specific analysis. Pre- and post-contrast high resolution relaxometry imaging and DCE-MRI were used for the pharmacokinetic analysis for the first time in NHP *in vivo*. Diffusion of gadolinium into the brain parenchyma, which otherwise does not cross the BBB, was used as a tracer to depict the BBB-opened areas. Quantitative analysis of $T_1$ relaxometry mapping and permeability was performed to detect and quantify, the volume of opening in the grey and white matter, the CA concentration, and the drug delivery efficiency in the two NHPs. The acoustic pressure dependence was also investigated. Finally, T2-weighted and Susceptibility Weighted Imaging (SWI) were performed in order to detect edema or hemorrhage.

## 2. Material and Methods

### 2.1. Animal Preparation

All procedures were approved by the Institutional Animal Care and Use Committee at Columbia University and the New York Psychiatric Institute. Two male rhesus macaques (*Macaca mulatta*) weighing 10 kg were used in this study. The animal handling was described elsewhere [3, 10]. For the entire procedure the animals were anesthetized with a mixture of oxygen and 2% isoflurane, while monitoring their vital signals. The animals' heart rate was kept around 110 heartbeats per minute and their respiratory rate was kept at 20 breaths per minute. Prior to sonication, the scalp hair was removed with a depilatory cream in order to ensure maximal acoustic transmission with minimum attenuation. For the FUS part the animal's head was placed in a stereotactic frame for targeting of ultrasound to

specific brain regions, using a manipulator and a positioning rod which indicated the focus relatively to the stereotactic coordinates, as shown in Figure 1.

### 2.2. Focused Ultrasound induced BBB opening

Two regions, the Caudate and the Putamen, with relevance to Parkinson's disease [11] were targeted transcranially with FUS in two (n=2) rhesus macaques, for a total of 32 sonications, 16 sonications each as shown in Figure 3(a). The targets were in one hemisphere and the contralateral side remained intact. The FUS setup as described elsewhere [12] consists of a single-element FUS transducer (H-107, Sonic Concepts, Bothell, WA) driven at 500 kHz with a focal size of 5.85 mm by 34 mm (−6dB) and a focal depth 62.2 mm, which overlapped with the targeted regions. The signal was generated by a function generator (model 33220A, Agilent Technologies Inc., Santa Clara, CA) amplified by a 50-dB amplifier (A075, Electronic Navigation Industries, Rochester, NY). The sonication acoustic pressure varied from 200 kPa to 600 kPa while the rest of the acoustic parameters remained the same (PRF: 2Hz, sonication duration: 120 s, pulse length: 10 ms). A bolus ($1.25 \times 10^8$ bubbles/kg) of manufactured in-house mono-disperse (4–5 μm in diameter), lipid-coated microbubbles[13] was administered intravenously in the beginning of the sonication.

### 2.3. Magnetic Resonance Imaging

Following sonication, as shown in Figure 2, the macaques were placed in the 3T MR scanner (Philips Medical Systems, Andover, MA, USA). 3D T2-weighted imaging (Turbo Spin Echo, TR/TE = 3000/80 ms; flip angle (FA): 90°; NEX= 3; spatial resolution: 1 × 1 × 2 $mm^3$) and 3D SWI (TR/TE = 19/27 ms; flip angle: 15°; NEX= 1; spatial resolution: 1 × 1 × 1 $mm^3$) sequences were acquired. The T2-w and the SWI acquisitions are performed for the detection of hyperintensity, i.e. edema, and/or hypointensity, i.e. hemorrhage respectively. Five pre- and post-CA injection, 3D Spoiled Gradient Echo (SPGR) / 3D T1 Fast field echo (FFE) images (FOV:16 cm, matrix 160×160, TR/TE: 20/5ms, FA: 5°, 10° 15° 20° 35°, NEX=2, 0.89 × 0.89 ×1 $mm^3$) were acquired and used for variable flip angle (VFA) based T1 relaxivity mapping, before and after intravenous injection of gadodiamide (Gd-DTPA-BMA, 0.2 ml/kg).The DCE-MRI sequence was acquired between the pre- and post-CA SPGR sequences. In total, 90 sets of 3D T1 FFE images were acquired at 15 s intervals (TR/TE: 4.2/1.7 ms; FA= 20°, resolution: 1×1×2.5 $mm^3$). At the beginning of the $6^{th}$ acquisition, a bolus of 0.2 mL/kg of Gd-DTPA-BMA (Omniscan®, GE Healthcare, Princeton, NJ, USA) was injected intravenously in the saphenous leg vein.

### 2.4. VFA-based T1 mapping

Based upon the Bloch equation[14], a steady-state MR signal intensity ($s_k$) acquired by a T1-weighted SPGR sequence with a flip angle (FA) $a_k$ (k=1,2,.., $N_{FA}$; $N_{FA}$ is the number of FAs) and a repetition time TR is given by:

$$s_k = \frac{M_o \sin a_k (1 - E)}{1 - E * \cos a_k}, \quad (1)$$

where $M_o$ is the equilibrium longitudinal magnetization, and $E= e^{(-TR/T1)}$. Pre and Post-contrast 3D SPGR images are processed off-line using an in-house algorithm developed in Matlab (The MathWorks, Inc., MA, USA). T1 and $M_0$ maps using the VFA method were generated by fitting the voxel-wise image intensities at Eq. [1] using polynomial curve fitting algorithm and $a_1$=5°, $a_2$=10°, $a_3$=15°, $a_4$=20° $a_5$=35°. The method was first validated in a phantom (Mahgphan® Quantitative Imaging Phantom) with known $T_1$ times as shown in Table 1.

### 2.5. DR1 mapping and BBB opening detection

An example of $T_{1,0}$ and $T_1$ maps as shown in Figure 3(b) and Figure 3(c), i.e. $T_1$ maps before and after MR-CA injection. $T_1$ decreases and is observed in the $T_1$ maps as hypointense voxels only in the BBB-disrupted areas as shown in Figure 3(c). After this step, R1 maps before and after the CA injection were also generated (R1=1/T1). Since $R_1$ relaxivity increases only where gadolinium diffuses, the ΔR1 maps, where

$$\Delta \mathrm{R1}=\mathrm{R1}_{\mathrm{post}}-\mathrm{R1}_{\mathrm{pre}},$$

were generated and used for the detection and quantification of the BBB opening, using the CA as a tracer for the BBB opening. A threshold of ΔR1 greater than 0.05 $s^{-1}$ was set for the detection of areas of gadolinium diffusion, which includes the diffusion through the opened BBB, as well as the vasculature. An example of the voxels that passed this threshold is shown in Figure 3(d).

### 2.6. Grey and white matter segmentation

Since grey matter (GM), white matter (WM), CSF etc. have distinctive characteristic $T_1$ times at a given field strength, $T_{1,0}$ mapping was used for GM and WM segmentation. The $T_1$ times of GM and WM were measured for both NHPs at 1330 ± 66 ms and 872 ± 78 ms respectively. The range for GM and WM segmentation was set around the mean value and ranging from 2.5 standard deviations below that to 2.5 standard deviations above that value. Therefore, voxels with $T_{1,0}$ of 677–1066 ms were assumed to belong to WM, and voxels with $T_{1,0}$ of 1165–1495 ms were assumed to belong to GM. The BBB opening voxels that belonged to the targeted areas where overlaid on a $T_{1,0}$ map in order to determine to which structure (GM or WM) in which it belonged was detected as shown in Figure 3(e). In that manner, the volume of opening ($V_{BBB}$) in the GM and WM were quantified.

### 2.7. Concentration mapping and delivery efficiency estimation

Magnetic resonance contrast agent concentration maps ([Gd]) were then calculated from the $T_{1,0}$ time before MR-CA injection and the $T_1$ time after MR-CA injection using [15]

$$[Gd]=\frac{1}{r_{Gd}}\left(\frac{1}{T_1}-\frac{1}{T_{1,o}}\right). \quad (2)$$

An example is shown in Figure 3(f). The gadolinium concentration $C_{Gd}$ was then converted to the mass amount of the CA delivered in the BBB opening area by multiplying with the

voxel volume, i.e. 0.89 mm × 0.89 mm × 1 mm = 0.79 $mm^3$ = 0.79 μL, since 1 mM= 1mmol/L. The total amount of gadolinium, i.e. Gd-DTPA-BMA, delivered to the brain through the BBB opening was therefore estimated. The amount of CA injected intravenously was also known, so the percentage of the amount of CA that was delivered to the BBB opening over the amount of CA that was injected in the bloodstream was measured and reported for delivery efficiency estimation.

### 2.8. Permeability mapping

The General Kinetic Model (GKM), and in particular the extended modified Tofts model[9], [16] was used to quantify the permeability in the NHP brain following the first order differential equation:

$$\frac{\mathrm{dC_t}(t)}{dt}=\mathrm{K_{trans}C}_P(t)-\mathrm{K_{ep}C}_t(t), \quad (3)$$

where $K_{trans}$ and $K_{ep}$ are the transfer rates from the blood plasma to the extravascular extracellular space (EES) and vice versa, $C_p(t)$ and $C_t(t)$ are the concentrations of Gd-DTPA-BMA in the blood plasma and EES respectively. The plasma concentration $C_P(t)$ is a fraction of the concentration in the blood $C_B(t)$ defined as $C_P(t)=(1-H_{ct})\ C_b(t)$, where $H_{ct}$ is the animal hematocrit. The $C_P(t)$ also provides the Arterial Input Function (AIF) which, following a bolus injection in the bloodstream, follows a bi-exponential decay of the form:

$$\mathrm{C}_P(t)=\mathrm{A}_1\mathrm{e}^{-m_1t}+\mathrm{A}_2\mathrm{e}^{-m_2t}, \quad (4)$$

where $A_1$,$A_2$ and $m_1$,$m_2$ are the amplitude and decay rates respectively. The AIF was fitted individually for each experiment in a custom algorithm in Matlab (MathWorks, Inc. Natick, MA, USA) in order to provide accurate and robust estimations for each case. Eq (4) is substituted in Eq.(3) which then can be expressed in the equivalent form:

$$\mathrm{C}_t(t)=\left(\frac{\mathrm{K_{trans}A_1}}{m_1-\mathrm{K_{ep}}}+\frac{\mathrm{K_{trans}A_2}}{m_2-\mathrm{K_{ep}}}\right)\mathrm{e}^{-K_{\mathrm{ep}}t}-\frac{\mathrm{K_{trans}A_1}}{m_1-\mathrm{K_{ep}}}\mathrm{e}^{-m_1t}-\frac{\mathrm{K_{trans}A_2}}{m_2-\mathrm{K_{ep}}}\mathrm{e}^{-m_2t} \quad (5)$$

The measured signal for the DCE-MRI T1-weighted images is converted to concentration using the Solomon-Bloembergen equation [17]:

$$[\mathrm{Gd}(t)]=\frac{s_{\mathrm{post}}(t)-s_{\mathrm{pre}}}{s_{\mathrm{pre}}\times T_{1,0}\times r_1}, \quad (6)$$

where the $T_{1,0}$ which is the longitudinal relaxation time of the voxel as measured using the VFA-bases T1 mapping technique mentioned earlier, $S_{post}$ (t) is the signal intensity at each repetition following gadolinium injection, and $S_{pre}$ is the signal intensity before the

injection. The $K_{trans}$ and $K_{ep}$ values at each voxel were conventionally estimated from the measured [Gd(t)] by a non-linear least squares (NLS) fitting

$$\Phi(\mathrm{K}_{\mathrm{trans}}, K_{\mathrm{ep}}) = \sum_{t=1}^{NR} (\mathrm{C}_t(t) - \mathrm{Gd}(t))^2, \quad (7)$$

where NR is the number of repetitions, i.e., 90, implementing a trust region reflective algorithm developed in Matlab (MathWorks, Inc. Natick, MA, USA). $K_{trans}$ and $K_{ep}$ maps were generated for the whole brain, to better visualize the opening in the FUS-targeted regions. The average $K_{trans}$ was also calculated in the entire $V_{BBB}$, as well as separately in the GM and WM.

### 2.9. Statistical Analysis

One-way analysis of variance (ANOVA) was performed for each NHP to compare the differences among different pressures for $V_{BBB}$, total Gd-DTPA-BMA amount delivered and $K_{trans}$. When the null hypothesis was rejected based on the ANOVA, a post-hoc statistical analysis was performed using Tukey's multiple comparisons test. This test was selected because it assumes independence of the observations being tested as well as equal variation across observations.

## 3. Results

An example of the BBB-opening in the Caudate and the Putamen of the left hemisphere of NHP 1, sonicated at 300 kPa is shown in Figure 4(a). The opening is not easily detected in the post- T1-w image. No edema or hemorrhage is detected in the T2-w and SWI respectively. $V_{BBB}$ is detected using the ΔR1 mapping and is shown in red overlaid on the $T_{1,0}$ map, revealing that it was mostly induced in the GM. The concentration map reveals the diffusion pattern, where higher [Gd] was detected in the GM mostly. Finally, the 3D permeability map reveals an increase in the sonicated areas only.

An example of the BBB opening in the Caudate of the right hemisphere of NHP 2, sonicated at 450 kPa is shown in Figure 4(b). The opening is not easily seen in the post-Gd T1-w image. No edema or hemorrhage is detected in the T2-w and SWI, respectively. $V_{BBB}$ is detected using the DR1 mapping and is shown in red overlaid on the $T_{1,0}$ map, revealing that it was mostly induced in the GM, interrupted by the WM. The concentration map reveals the diffusion pattern, where lower [Gd] was detected than in Figure 4(a) and NHP 1. Finally, the 3D permeability map reveals an increase in the sonicated area only, while it was mainly contained in the GM areas.

Two examples of two different pressures, at 200 kPa and 400 kPa respectively, are shown in Figure 5 for NHP 1. This animal subject responded to the increase in acoustic pressure different than NHP 2. As shown here, at 200 kPa a relatively small opening was induced, and the concentration in the disrupted area remained low. With the increase to 400 kPa, however, the volume increased significantly, and in some areas gadolinium concentration reached high values too, especially compared to 300 kPa shown in Figure 4(a). As shown in

the concentration maps, for both pressures, gadolinium concentration is higher and mainly contained in grey matter, compared to white matter.

Quantitative measurements of the volume of opening ($V_{BBB}$) in NHP 1 and NHP 2, along with the GM and WM segmentation are shown in Figure 6(a) and (b). $V_{BBB}$ in NHP 2, as shown here, was lower than the $V_{BBB}$ in NHP 1 for the pressures tested. Following subject-specific analysis, in NHP 1, ANOVA revealed statistically significant differences among the groups, and in particular significant difference ($p<0.01$) was detected between the lowest pressure (200 kPa) and the medium pressure (300 kPa), while an even larger difference ($p<0.001$) was detected between the lowest and the highest pressure (600 kPa). The $V_{BBB}$ was increased in the GM, compared to the WM. In NHP 2, ANOVA did not reveal any statistically significant differences among the three acoustic pressures used.

The total amount of gadolinium (Gd-DTPA-BMA) detected in the GM and the WM is shown in Figure 6(c) for NHP 1 and Figure 6(d) for NHP 2. The subject specific analysis for NHP 1, revealed a statistically significant difference of $p<0.001$ and $p<0.0001$ between the lowest pressure and the medium and highest pressures, respectively. There was also significant difference ($p<0.05$) between the medium and the highest pressure amplitude. In NHP 2, the only significance ($p<0.05$) in the total amount of gadolinium delivered to the BBB opening was detected between the lowest and the highest pressure.

Boxplots of the average $K_{trans}$ measured in both the GM and WM for all pressures used for NHP 1 and NHP 2 are shown in Figure 6 (e) and (f), respectively. The far left side shows the background permeability of the brain in GM and WM. On average, the permeability in the GM after BBB disruption was higher than the permeability in the WM by $1.29 \pm 0.23 * 10^{-4}$/s, while they both increased with acoustic pressure. Similarly, following subject-specific analysis, the average $K_{trans}$ was greater in NHP 1 than in NHP 2.

The total amount of Gd-DTPA-BMA for all PNP and both NHPs are shown together in Figure 6(g). The amount delivered at the lowest PNP for NHP 1, i.e., 200 kPa, was not significantly different from the amount delivered at the lowest PNP for NHP 2, i.e., 300 kPa. However, at 300 kPa there was a significantly larger amount delivered in NHP 1 than in NHP 2, for both the caudate and the putamen. The amount delivered in NHP 1 increased rapidly with PNP, but for NHP 2 the slope was lower. The average increase in permeability for all PNPs in both NHPs is shown in Figure 6(h). It increased with pressure but no significant differences were detected.

Scatter plots of Gd-DTPA-BMA versus $V_{BBB}$ and $K_{trans}$ are shown in Figure 7(a) and (b), respectively. Subject-specific analysis for the Gd-DTPA-BMA and $V_{BBB}$ correlation, a linear regression showed a correlation of $R^2=0.71$ for NHP 1, and $R^2=0.37$ for NHP 2. Combining the results from both the NHPs, the $R^2$ was measured equal to 0.70. No linear correlation was detected between Gd-DTPA-BMA and $K_{trans}$.

The amount of Gd-DTPA-BMA delivered for all PNPs and NHPs is summarized in Table 2, along with the delivery efficiency estimation. Efficiency was increased with pressure; however, it was different for the two NHPs. It ranged from $0.0007 \pm 0.0001\%$ to 0.0043

± 0.0003% for NHP1, and was much lower for NHP2 ranging from 0.0005 ± 0.0001% to 0.0016 ± 0.0003%.

## 4. Discussion

In this study, a subject-specific pharmacokinetic and pharmacodynamic analysis was performed in order to characterize the physiologic changes and the delivery efficiency in two non-human primates following the FUS-induced BBB opening in vivo. The acoustic pressure was varied in order to investigate the effects of this parameter and design an optimal and efficient drug delivery treatment plan. The volume of BBB opening, the amount of model drug delivered and the permeability increased with the acoustic pressure. However, the increase was more profound in one NHP compared to the other, indicating the effect of individual differences in the outcome of the treatment.

A major innovation in this study is the introduction of quantitative MR relaxometry techniques, i.e. DR1 mapping, for the detection and characterization of BBB opening. Previously, pre- and post- contrast T1-weighted imaging has been used for detection of BBB opening in NHP, with arbitrary opening detection thresholds, which may induce further variability and discrepancy in results among different studies and experiments. The methods and analysis implemented here provide a robust protocol for detection of BBB opening, user-independent, along with quantitative information with high spatial resolution. The MR sequences and algorithms for data processing were also validated in phantoms (Table 1), in order to safely report accurate quantitative measurements. Segmentation of grey and white matter Figure 3(b), based upon their distinctive $T_1$ relaxation times and quantification of the opening volume in each of them individually was reported in this study for the first time, revealing further insights to the effect of the FUS-application to the highly inhomogeneous brain.

MR-contrast agent concentration mapping and permeability mapping have been previously used for brain studies in rodents [6], [7], [18]. However, it is used here for the first time in NHP, and additionally, the delivery efficiency was estimated following a three-dimensional analysis. First, this study provides an important feedback in a the clinical application of the FUS-induced BBB opening, since the ultimate goal is drug delivery in therapeutically relevant doses. Second, it constitutes an *in vivo* tool for studying drug delivery efficiency, indirectly and non-invasively; this is a major advantage compared to other techniques that are used for the same purpose such as protein quantification in excised brains *post-portem*, or PET/CT in conjunction with the injection of radio-labelled molecules. Gadolinium Gd-DTPA-BMA is used in this study as a model drug and it has relatively low molecular weight (574 Da), thus, the delivery efficiency and permeability may be different using different drugs with higher molecular weights, different half-life, apparent diffusion coefficient etc. Nevertheless, the trend and patterns shown onto the maps can still be used for qualitative as well as statistical analysis for optimization of the acoustic parameters in order to achiever efficient and safe drug delivery.

The subject-specific analysis of this study was due to the difference in the effect of acoustic pressure between the two NHPs, which belong to the same species, have the same age and

weight, and which was a very interesting finding. Consistently, NHP 1 had larger volumes of opening, higher amount of Gd-DTPA-BMA delivered, and slightly higher average permeability than NHP 2 (Figure 6). For these reasons, different pressures were selected for the two NHPs, based on their acoustic pressure opening threshold, which was studied before selecting the parameters shown in this study. For NHP 1, the lowest pressure used was 200 kPa, compared to 350 kPa which was the lowest pressure used for NHP 2. Also, the highest pressure used for NHP 1 was 400 kPa, and was shown to cover the entire area of interest. For NHP 2, the highest pressure used was 600 kPa and the same amount of opening volume was never reached.

For NHP 1, significant difference was detected between the lowest acoustic pressure and the each of the higher pressures in the opening volume Figure 6. Significant differences were detected among all different pressures in the amount of Gd-DTPA-BMA delivered. These findings indicate that the volume of opening might have reached a plateau at the higher pressures, whereas the amount of Gd-DTPA-BMA delivered continued to increase with pressure. The average $K_{trans}$ did not significantly vary with acoustic pressure; however, it is significantly increased compared to the sham group. It could thus be hypothesized, as previously reported [6], that the average $K_{trans}$ might be underestimating the effect of permeability change in the brain and might not be as a reliable quantitative indicator.

For NHP 2, no significant differences were detected in the volume of opening among the groups with different acoustic pressures used Figure 6. Significance between the lowest and the highest acoustic pressure was detected in the amount of Gd-DTPA-BMA though. NHP 2 had consistently lower opening volumes etc than NHP 1. Inherently, the permeability of the sham experiments in NHP 2 was slightly lower than in NHP 1, which could be one possible explanation as to why NHP 2 was more “resistant” to BBB opening. Furthermore, the shape and the thickness of the NHPs’ skulls are not identical, as it can also be seen in their respective MRI coronal sections shown here. This variation may simulate the differences among different individuals that should be expected in a clinical setting. The incidence angle, along with aberration effects could be another reason why higher acoustic pressures were required in NHP 2; factors that are currently being analyzed by the group and will be reported independently.

Overall, the permeability change maps in this study were very distinct compared to the respective maps in rodents[4], [6], [18] which almost followed a two-dimensional Gaussian distribution around the focal spot. In this study, the permeability was found to be increased towards the center of the target, i.e. the center of the focus, where the peak negative pressure is also higher than in the outer part, but it was not uniform. It followed the underlying anatomical details and physiology. The permeability unit in those studies was $min^{-1}$, whereas in this study $s^{-1}$ was used. The lowest permeability increase in the current study in NHP was around 0.0001 $s^{-1}$, which equals to 0.006 $min^{-1}$, while the permeability threshold in mice was reported at 0.005 $min^{-1}$ [18]. Therefore, the lowest permeability detected in NHPs here was very similar to what was found in mice using FUS. The highest permeability increase in NHPs was 0.00047 $s^{-1}$ or 0.028 $min^{-1}$; while in mice the permeability was found to increase with pressure up to a plateau with similar permeability with a muscle which was

reported at 0.048 $min^{-1}$. Therefore, the same plateau was not reached here; the maximum increased was at 58% of this plateau, in NHPs.

Despite the offset between the two NHP's and the different outcomes with the acoustic pressure, there were also some common findings. Firstly, BBB opening was mainly contained within the grey matter, and in many cases it was shown to be discontinued in the white matter. At the same time, white matter was measured to be less permeable than grey matter, which could be a possible explanation for this phenomenon. White matter is known to be less vascular than grey matter [19], therefore it could be hypothesized that lower microbubble perfusion also resulted in a lower number of cavitation nuclei, hence a reduced BBB opening. Similarly, a reduced amount of Gd-DTPA-BMA was capable of reaching the white matter and diffuses through the disrupted BBB.

Furthermore, only in NHP1 a good correlation was found between the amount of Gd-DTPA-BMA delivered and the volume of opening $V_{BBB}$. NHP exhibited better agreement when a linear regression was tested, with higher correlation than NHP2, although, when combined, $R^2$ remained pretty high and equal to 0.70 (Figure 6). No correlation was found between the amount of gadolinium delivered and the average increase in permeability. These findings imply that the amount of drug delivered linearly increased with the volume of opening, while the average permeability change was not deemed reliable indicator for the amount of drug that could be delivered.

Finally, the delivery efficiency showed that the percentage was very low for both NHP's yet within the clinical relevant dose (Table 2)[20]. Here, we were able to deliver up to 20 μg of gadolinium with the use of FUS when targeting the putamen, and the experiments were performed biweekly in each monkey. These findings suggest the high potential of this technique for the treatment of neurodegenerative diseases.

## 5. Conclusions

In this study, a subject-specific analysis of the FUS-induced BBB opening in NHPs was performed, using pharmacokinetic analysis in order to further investigate the physiologic changes in the brain and their correlation to their anatomy. Permeability mapping, concentration mapping and drug delivery dose were measured *in vivo* in NHPs for the first time, in order to assess the efficiency of the FUS-induced BBB opening as a technique with therapeutic potential in the treatment of neurodegenerative diseases. Relaxometry techniques were used for the robust quantitative detection of the BBB opening as well as the grey and white matter segmentation. Overall, the volume of opening was greater in the grey matter and mainly contained there, compared to the white matter, which was also shown to be less permeable. The contrast agent's diffusion patterns revealed important information of the FUS-induced BBB opening following the patterns of the underlying brain structures. The FUS-induced drug delivery increased with the acoustic pressure used. The dose of Gd delivered to the brain parenchyma remained within the 1–25 μg range with the acoustic parameters used in this study, which has been shown to be a clinically relevant dose for brain applications.

## Acknowledgments

**Funding Sources**

This work was supported by the National Institutes of Health (R01AG038961 and R01EB009041), the Focused Ultrasound Surgery foundation and the W.H. Coulter foundation.

## References

1. Tung YS, Marquet F, Teichert T, Ferrera VP, Konofagou EE. Feasibility of noninvasive cavitation-guided blood-brain barrier opening using focused ultrasound and microbubbles in nonhuman primates. Appl Phys Lett. 2011; 98(16):163704. [PubMed: 21580802]
2. McDannold N, Arvanitis CD, Vykhodtseva N, Livingstone MS. Temporary disruption of the blood-brain barrier by use of ultrasound and microbubbles: safety and efficacy evaluation in rhesus macaques. Cancer Res. 2012; 72(14):3652–3663. [PubMed: 22552291]
3. Marquet F, Tung YS, Teichert T, Ferrera VP, Konofagou EE. Noninvasive, transient and selective blood-brain barrier opening in non-human primates in vivo. PloS One. 2011; 6(7):22598.
4. Vlachos F, Tung YS, Konofagou EE. Permeability assessment of the focused ultrasound-induced blood-brain barrier opening using dynamic contrast-enhanced MRI. Phys Med Biol. 2010; 55(18): 5451–5466. [PubMed: 20736501]
5. Samiotaki G, Vlachos F, Tung YS, Konofagou EE. A quantitative pressure and microbubble-size dependence study of focused ultrasound-induced blood-brain barrier opening reversibility in vivo using MRI. Magn Reson Med. 2011; 67(3):769–777. [PubMed: 21858862]
6. Samiotaki G, Konofagou EE. Dependence of the reversibility of focused- ultrasound-induced blood-brain barrier opening on pressure and pulse length in vivo. IEEE Trans Ultrason Ferroelectr Freq Control. 2013; 60(11):2257–2265. [PubMed: 24158283]
7. Marty B, Larrat B, Van Landeghem M, Robic C, Robert P, Port M, Le Bihan D, Pernot M, Tanter M, Lethimonnier F, Mériaux S. Dynamic study of blood-brain barrier closure after its disruption using ultrasound: a quantitative analysis. J Cereb Blood Flow Metab Off J Int Soc Cereb Blood Flow Metab. 2013; 32(10):1948–1958.
8. Fram EK, Herfkens RJ, Johnson GA, Glover GH, Karis JP, Shimakawa A, Perkins TG, Pelc NJ. Rapid calculation of T1 using variable flip angle gradient refocused imaging. Magn Reson Med. 1987; 5(3):201–208. [PubMed: 3431390]
9. Tofts PS, Kermode AG. Measurement of the blood-brain barrier permeability and leakage space using dynamic MR imaging. 1. Fundamental concepts. Magn Reson Med. 1991; 17(2):357–367. [PubMed: 2062210]
10. Tung YS, Marquet F, Teichert T, Ferrera VP, Konofagou EE. Feasibility of noninvasive cavitation-guided blood-brain barrier opening using focused ultrasound and microbubbles in nonhuman primates. Appl Phys Lett. 2011; 98(16):163704. [PubMed: 21580802]
11. Blesa J, Przedborski S. Parkinson’s disease: animal models and dopaminergic cell vulnerability. Front Neuroanat. 2014; 8:155. 2014. [PubMed: 25565980]
12. Wu SY, Tung YS, Marquet F, Downs M, Sanchez C, Chen C, Ferrera VP, Konofagou EE. Transcranial cavitation detection in primates during blood-brain barrier opening-a performance assessment study. IEEE Trans Ultrason Ferroelectr Freq Control. 2014; 61(6):966–978. [PubMed: 24859660]
13. Feshitan JA, Chen CC, Kwan JJ, Borden MA. Microbubble size isolation by differential centrifugation. J Colloid Interface Sci. 2009; 329(2):316–324. [PubMed: 18950786]
14. Zur Y, Stokar S, Bendel P. An analysis of fast imaging sequences with steady-state transverse magnetization refocusing. Magn Reson Med. 1988; 6(2):175–193. [PubMed: 3367775]
15. Swift TJ, Connick RE. NMR-Relaxation Mechanisms of O17 in Aqueous Solutions of Paramagnetic Cations and the Lifetime of Water Molecules in the First Coordination Sphere. J Chem Phys. 1962; 37(2):307–320.
16. Tofts PS, Brix G, Buckley DL, Evelhoch JL, Henderson E, Knopp MV, Larsson HB, Lee TY, Mayr NA, Parker GJ, Port RE, Taylor J, Weisskoff RM. Estimating kinetic parameters from dynamic

contrast-enhanced T(1)-weighted MRI of a diffusable tracer: standardized quantities and symbols. Magn Reson Med. 1999; 10(3):223–232.

17. Parker, GJM., Buckley, DL. Tracer Kinetic Modelling for T1-Weighted DCE-MRI. In: Jackson, A.Buckley, DL., Parker, GJM., editors. Dynamic Contrast-Enhanced Magnetic Resonance Imaging in Oncology. Berlin Heidelberg (Germany): Springer-Verlag; 2005. p. 81-92.
18. Vlachos F, Tung YS, Konofagou EE. Permeability dependence study of the focused ultrasound-induced blood-brain barrier opening at distinct pressures and microbubble diameters using DCE-MRI. Magn Reson Med. 2011; 66(3):821–830. [PubMed: 21465543]
19. Kolb, B., Whishaw, IQ. Fundamentals of Human Neuropsychology. 6th. NY: Macmillan; 2009.
20. Grondin R, Zhang Z, Ai Y, Ding F, Walton AA, Surgener SP, Gerhardt GA, Gash DM. Intraputamenal infusion of exogenous neurturin protein restores motor and dopaminergic function in the globus pallidus of MPTP-lesioned rhesus monkeys. Cell Transplant. 2008; 17(4):373–381. [PubMed: 18522240]

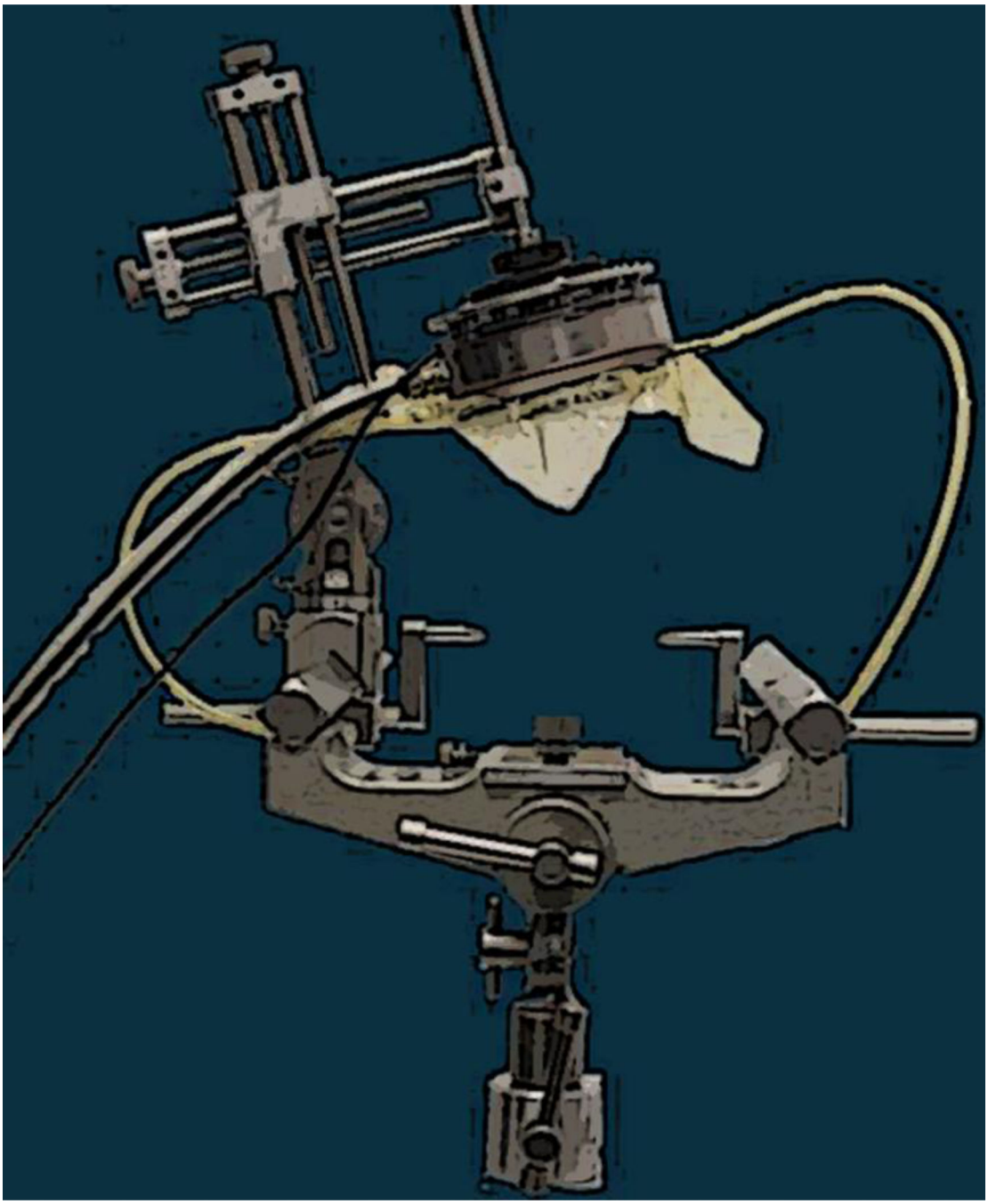

**Figure 1.**
FUS experimental setup. Targeting is based on stereotactic coordinates that correspond to atlas coordinates.

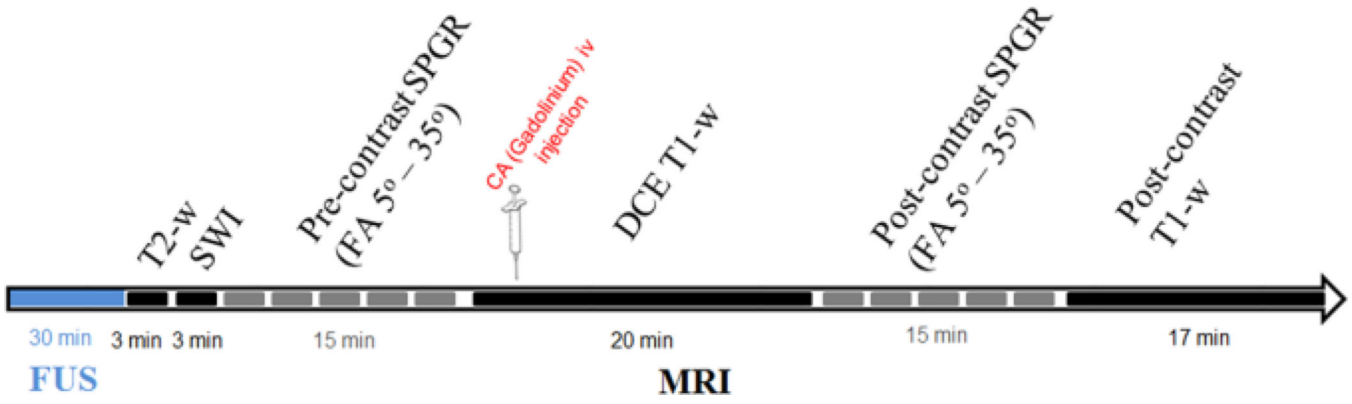


**Figure 2.**
Experimental timeline. FUS is performed outside the MRI.

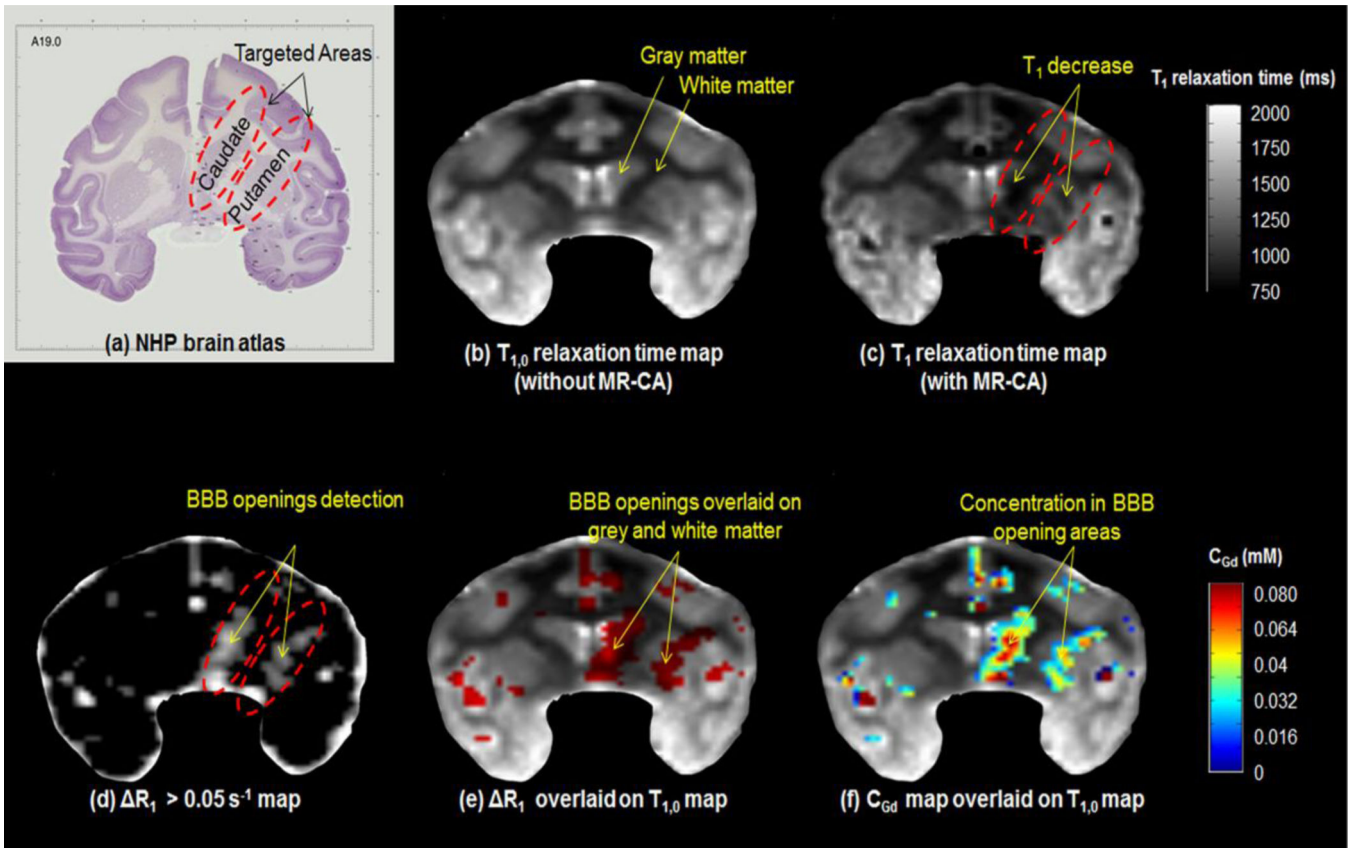


**Figure 3.**

In (a) the targeting on Caudate and Putamen in a brain atlas is shown. (b)$T_{1,0}$ relaxation times map before contrast agent injection and (c) T1 relaxation times map after contrast agent injection. (d) The voxels that are satisfied the ΔR1 > 0.05 s−1 threshold criterion are red and are depicting only the brain areas where gadolinium diffused; apart from the BBB-opening area gadolinium also appears in the vasculature. (e) The voxels of ΔR1 are overlaid on $T_{1,0}$ map in order to visualize the BBB in the gray matter (GM) and white matter (WM). In (d) gadolinium concentration map $C_{Gd}$ is shown, overlaid again on the T1,0 map in order to visualize the $C_{Gd}$ in the GM and WM. Most of the VBBB was detected in the GM, along with higher $C_{Gd}$ in these areas.

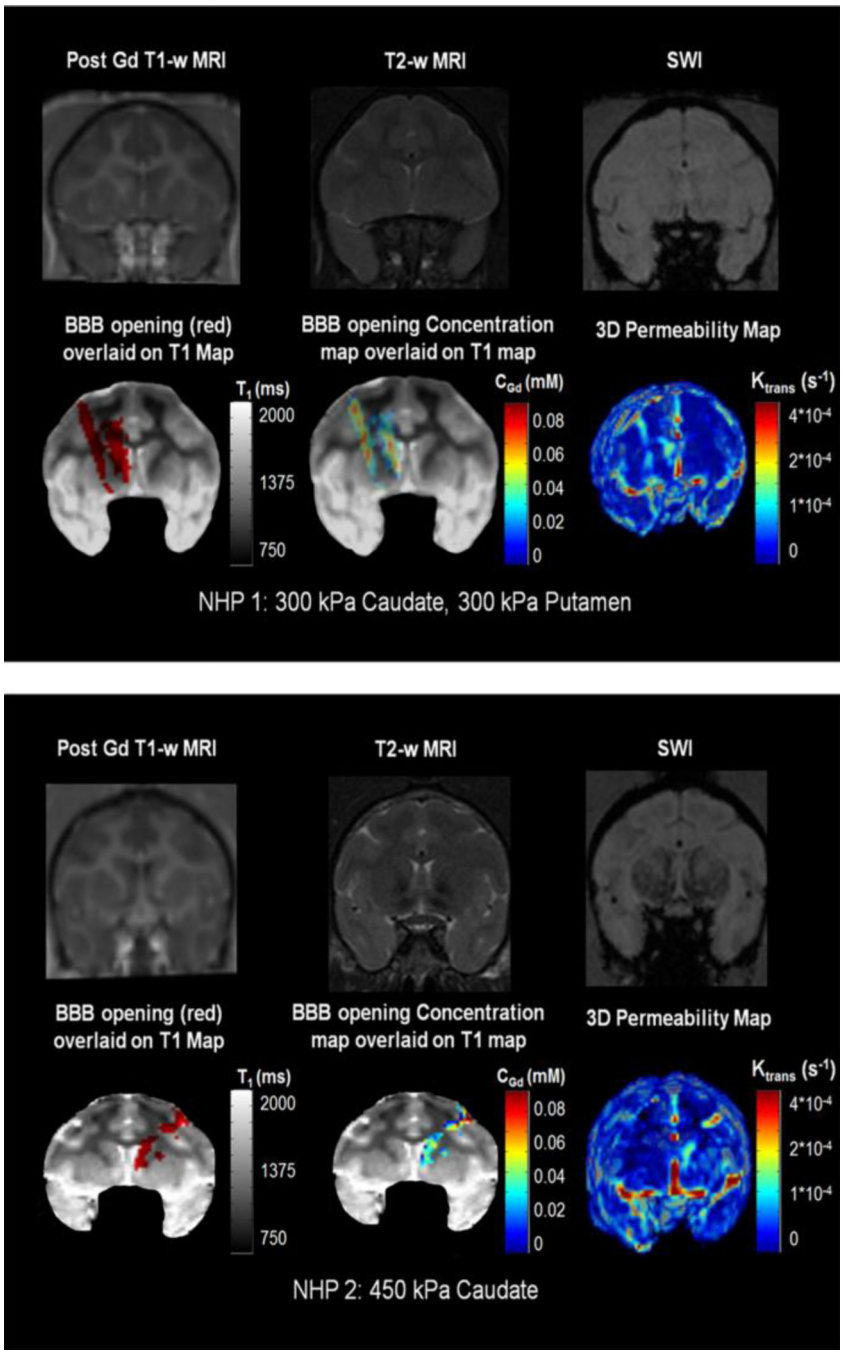


**Figure 4.**

Example of the BBB-opening in the Caudate and the Putamen of the left hemisphere of NHP 1, sonicated at 300 kPa. Example of the BBB-opening in the Caudate of the right hemisphere of NHP 2, sonicated at 450 kPa.

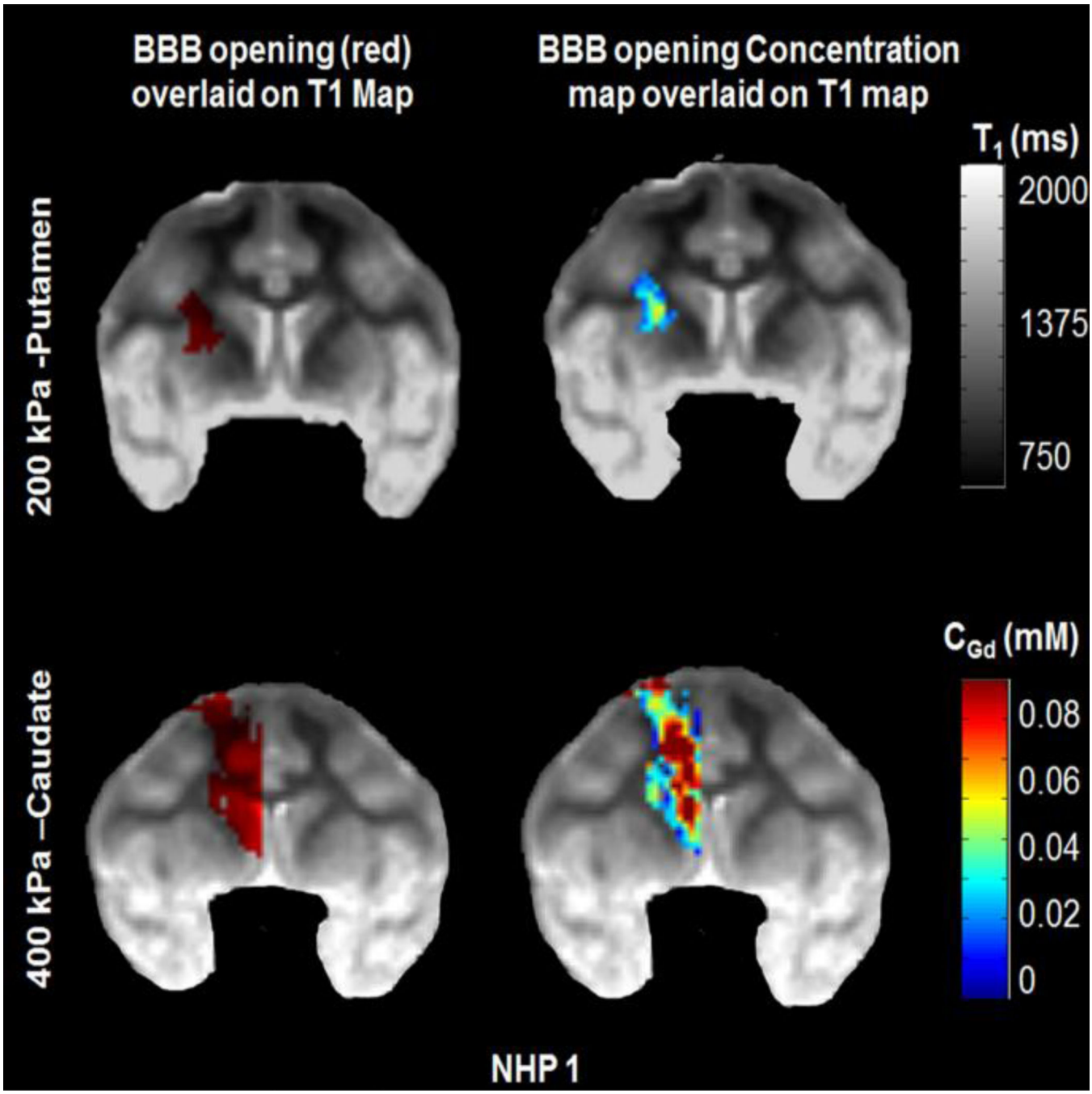


**Figure 5.**

Example from NHP 1 from two different pressures, 200 kPa and 400 kPa. The increase of pressure resulted in increase of the opening volume as well as the increase of gadolinium concentration. Gadolinium concentration is higher and mainly contained in the grey matter.

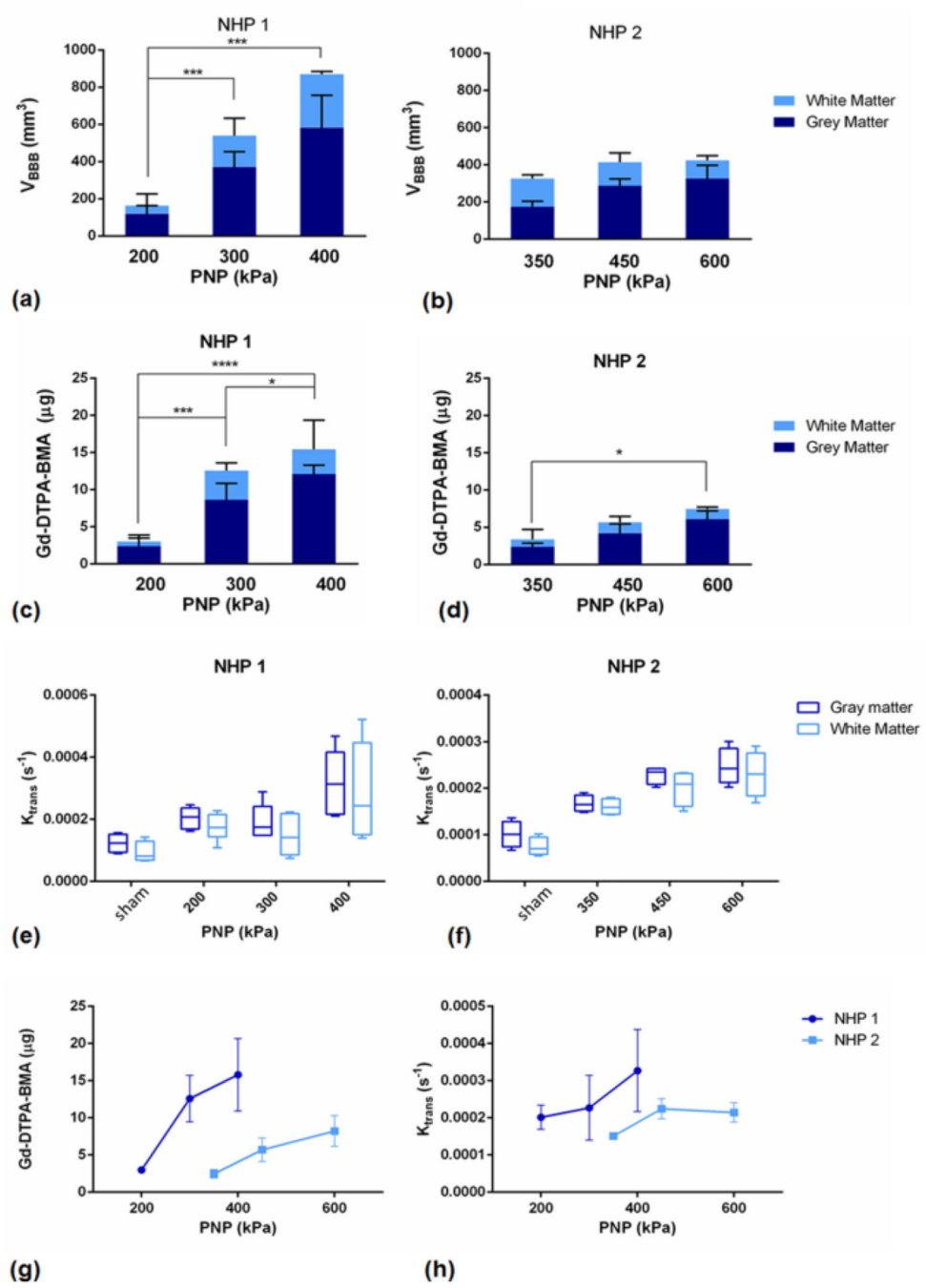


**Figure 6.**

Volume of opening ($V_{BBB}$) in NHP 1 in the GM and WM. Two asterisks (**) denote $p<0.01$, three asterisks (***) denote $p<0.001$ and was detected between the lowest and the highest pressure (600 kPa). $V_{BBB}$ was increased in the GM, compared to the WM. (b) $V_{BBB}$ in NHP 2 is shown, in the GM and WM. (c) Total amount of gadoloinium (Gd-DTPA-BMA) in NHP 1, divided in the amount detected in the GM and the WM, and in NHP 2 in (d). (e) Boxplots of the average $K_{trans}$ in NHP 1, showing the background $K_{trans}$ of the brain in the GM and WM, and in NHP 2 in (f).

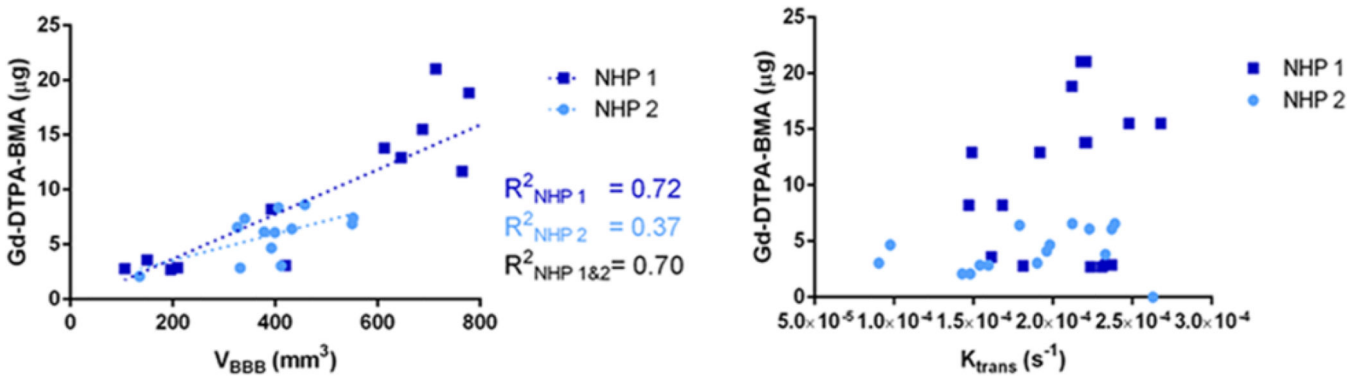


**Figure 7.**
Correlation between Gd-DTPA-BMA and $V_{BBB}$ and (b) $K_{trans}$.

**Table 1**

Phantom Testing

| Sample # | Actual T1 time (ms) | Measured T1 time (ms) |
|---|---|---|
| **1** | 450 | 460 ± 37 |
| **2** | 600 | 619 ± 48 |
| **3** | 900 | 897 ± 24 |
| **4** | 700 | 750 ± 36 |

**Table 2**

Delivery efficiency estimation

| NHP 1 | | | NHP 2 | | |
|---|---|---|---|---|---|
| **PNP** | **Amount delivered (μg)** | **Delivery efficiency (%)** | **PNP** | **Amount delivered (μg)** | **Delivery efficiency (%)** |
| **200** | 2.99 ± 0.42 | 0.0007 ± 0.0001 | **300** | 2.47 ± 0.55 | 0.0005 ± 0.0001 |
| **300** | 9.18 ± 5.84 | 0.0022 ± 0.0012 | **450** | 5.71 ± 1.58 | 0.0012 ± 0.0003 |
| **400** | 19.93 ± 1.56 | 0.0043 ± 0.0003 | **600** | 7.22 ± 1.27 | 0.0016 ± 0.0003 |